

Carbonyl Vibrational Wave Packet Circulation in $\text{Mn}_2(\text{CO})_{10}$ Driven by Ultrashort Polarized Laser Pulses

Mahmoud K. Abdel-Latif^{1,2} and Oliver Kühn^{1, a)}

¹⁾*Institut für Physik, Universität Rostock, D-18051 Rostock, Germany*

²⁾*Chemistry Department, Faculty of Science, Beni-Suef University, Beni-Suef, Egypt*

(Dated: 26 January 2013)

The excitation of the degenerate E_1 carbonyl stretching vibrations in dimanganese decacarbonyl is shown to trigger wave packet circulation in the subspace of these two modes. On the time scale of about 5 picoseconds intramolecular anharmonic couplings do not cause appreciable disturbance, even under conditions where the two E_1 modes are excited by up to about two vibrational quanta each. The compactness of the circulating wave packet is shown to depend strongly on the excitation conditions such as pulse duration and field strength. Numerical results for the solution of the seven-dimensional vibrational Schrödinger equation are obtained for a density functional theory based potential energy surface and using the multi-configuration time-dependent Hartree method.

I. INTRODUCTION

Recently, considerable attention has been paid to the excitation of degenerate electronic and vibrational states using circularly polarized laser light. Manz and coworkers have been the first to focus on the possibility of the excitation of electronic ring currents by laser-triggered formation of time-dependent hybrid states, e.g. in a Mg-porphyrin model^{1,2} as well as in the diatomic AlCl .³ A particularly interesting aspect has been the accompanying generation of giant magnetic fields.⁴ Subsequently, this work was extended to the vibrational domain in the electronic ground state. Here, degenerate bending vibrations of linear triatomic species such as $^{114}\text{CdH}_2$ ⁵ and FHF^- ⁶ have been excited to yield unidirectional pseudorotations. In contrast to previous work on the pseudorotation of Na_3 in the electronic B state excited by linearly polarized light,⁷ unidirectionality is achieved by circular polarization.

The present contribution is motivated by the question whether the dynamics of degenerate vibrations can be driven in more complex molecules, where one has to compete with intramolecular vibrational energy redistribution.⁸ Promising candidates are metal-carbonyl compounds due to the strong and spectrally distinct infrared (IR) absorption of the carbonyl stretching vibrations. Previous studies of metal-carbonyl compounds have been focused especially on laser-driven CO vibrational ladder climbing.^{9–11} A particularly interesting example has been the experimental demonstration of ladder climbing up to the $\nu_{\text{CO}} = 6$ state in carboxyhemoglobin by Joffe and coworkers.¹¹ For this example, Meier and Heitz have developed a non-reactive gas phase model to simulate the excitation dynamics by using local control theory.¹² It should be noted, however, that the main goal of the experiment had been to achieve con-

trolled metal-carbonyl bond breaking assisted by anharmonic couplings between the initially excited CO mode and the metal-CO bond. A quantum dynamics study employing a reactive model provided support for the experimental finding that this anharmonic coupling is too weak to cause bond breaking on the time scale of a few picoseconds.^{13,14} The lack of sufficient anharmonic metal-CO coupling has also been found in the related model study of $\text{MnBr}(\text{CO})_5$ using a three-dimensional reactive Hamiltonian.¹⁵ Further experimental progress in vibrational ladder climbing has been reported in Ref. 16 where an evolutionary algorithm was used for pulse shaping such as to highly excite a CO mode in $\text{W}(\text{CO})_6$.

In the following we will consider dimanganese decacarbonyl $\text{Mn}_2(\text{CO})_{10}$ (cf. Fig. 1) as a model system. In the past it was in particular the photochemistry of $\text{Mn}_2(\text{CO})_{10}$ that attracted most attention (see, e.g., Ref. 17 and references cited therein). More recently, the prospect of having ten coupled carbonyl vibrations attracted the interest of two-dimensional IR spectroscopists.^{18–21} This included in particular a detailed investigation of the coupled CO fundamental and low-order overtone and combination tone vibrations using anharmonic vibrational perturbation theory for the subset of CO modes, which were treated by anharmonic couplings up to the fourth order.¹⁹ The anharmonic level shifts for all CO vibrations were found to be below 10 cm^{-1} .

In Section II A we will present results on the quantum chemical characterization of the global minimum structure of the $\text{Mn}_2(\text{CO})_{10}$ model system. Based on this structure we will develop a seven-dimensional (7D) model Hamiltonian in Section II B, which is designed such as to describe the dynamics of the two degenerate E_1 CO vibrational normal modes and their anharmonic coupling to the remaining degrees of freedom, which will be called a bath. Further, we will comment on the numerical solution of the time-dependent Schrödinger equation, which is done using the multiconfiguration time-dependent Hartree (MCTDH) approach to wave packet

^{a)}Electronic mail: oliver.kuehn@uni-rostock.de

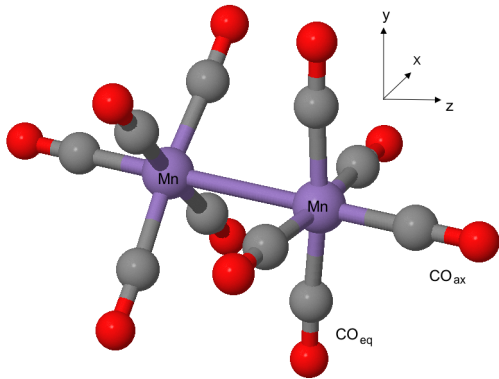


FIG. 1. Optimized D_{4d} structure of $Mn_2(CO)_{10}$ using DFT/BP86 with a TZVP basis set.

dynamics.^{22,23} Numerical results on the laser-driven dynamics will be discussed in Section III and conclusions are present in Section IV.

II. THEORY

A. Characterization of the Equilibrium Geometry

The structure of $Mn_2(CO)_{10}$ (cf. Fig. 1) has been optimized under D_{4d} symmetry constraint employing Density Functional Theory (DFT) with the BP86 functional and a triple zeta (TZVP) basis set as implemented in the Gaussian 03 program package.²⁴ Available crystal structure data are well reproduced as seen from the comparison given in Tab. I.

The stationary points were further characterized by a normal mode frequency analysis. The results for the IR active CO stretching vibrations are summarized in Tab. II. Overall, the agreement with experiment is quite rea-

| | calc. | Ref. 25 | Ref. 26 | Ref. 27 |
|------------------------|-------|---------|---------|---------|
| Mn-Mn | 2.97 | 2.92 | 2.98 | 2.90 |
| Mn-CO _{ax} | 1.81 | 1.73 | 1.80 | 1.82 |
| Mn-CO _{eq} | 1.85 | 1.83 | 1.87 | 1.86 |
| C-O _{ax} | 1.16 | 1.16 | 1.15 | 1.15 |
| C-O _{eq} | 1.15 | 1.16 | 1.15 | 1.14 |
| Mn-Mn-CO _{eq} | 86.8 | 86.2 | 86.6 | 86.1 |

TABLE I. Comparison between calculated geometrical parameters of the D_{4d} stationary point of $Mn_2(CO)_{10}$ and crystal structure data (bond lengths in Å, bond angles in degrees).

sonable even at the level of the harmonic approximation. Moreover, comparison with Ref. 19 indicates, that there is only a small dependence on the basis set (double vs. triple zeta).

B. Model Hamiltonian and Equations of Motion

The potential energy surface has been expressed in terms of normal mode coordinates, i.e. $V = V(\mathbf{Q}, \mathbf{q})$. Thereby, the two normal mode displacement coordinates describing the degenerate E_1 modes $\mathbf{Q} = (Q_1, Q_2)$, which are treated beyond harmonic approximation, have been separated from the remaining $3N - 8$ harmonic bath modes \mathbf{q} . The coupling, $V_c(\mathbf{Q}, \mathbf{q})$, between both sets of coordinates is modeled in linear order with respect to \mathbf{q} . Neglecting any contributions from global rotations the molecular Hamiltonian becomes

$$H_{\text{mol}} = H_{\mathbf{Q}} + H_{\mathbf{q}} + V_c(\mathbf{Q}, \mathbf{q}), \quad (1)$$

with the part describing the anharmonic coordinates

$$H_{\mathbf{Q}} = \frac{1}{2}(P_1^2 + P_2^2) + V(\mathbf{Q}, \mathbf{q} = 0), \quad (2)$$

the harmonic bath part

$$H_{\mathbf{q}} = \frac{1}{2} \sum_i (p_i^2 + \omega_i^2 q_i^2), \quad (3)$$

and the interaction

$$V_c(\mathbf{Q}, \mathbf{q}) = \frac{\partial V(\mathbf{Q}, \mathbf{q} = 0)}{\partial \mathbf{q}} \mathbf{q} = -\mathbf{F}(\mathbf{Q}) \mathbf{q}. \quad (4)$$

For $Mn_2(CO)_{10}$ there are 58 bath modes, but not all of them will couple appreciably to the \mathbf{Q} modes. Using the forces $\mathbf{F}(\mathbf{Q})$ the reorganization energy has been calculated according to the assumption that the frequencies do not change, i.e. $E_i^{(\text{reorg})} = [F_i(\mathbf{Q})/\omega_i]^2$.⁸ This quantity has been averaged on the \mathbf{Q} grid and the result is used to select the most relevant bath modes. The cut-off for the selection has been chosen such that modes whose averaged reorganization energy is substantially smaller than their harmonic frequencies are neglected. This gave a total of five relevant bath modes, which are combined

| mode | polariz. | calc. | exp. ²⁸ | exp. ²⁹ | calc. ¹⁹ |
|----------------|----------|-------------|--------------------|--------------------|---------------------|
| B ₂ | z | 1988 (788) | 1983 | 1992 | 1981 |
| E ₁ | (x,y) | 2014 (2224) | 2014 | 2025 | 2005 |
| B ₂ | z | 2045 (1348) | 2045 | 2053 | 2036 |

TABLE II. Comparison between calculated (harmonic, not scaled) and measured (Ref. 29 in gas phase, Ref. 28 in *n*-hexane) frequencies of IR active carbonyl stretching vibrations (in cm^{-1}). Calculated IR intensities are given in parenthesis (in km/mol).

TABLE III. Most important bath modes according the averaged reorganization energy $\langle E^{(\text{reorg})} \rangle$ (average over the full \mathbf{Q} grid and - in parentheses - over a reduced grid from -1 to 1 $a_0(\text{a.m.u.})^{1/2}$). The parameters of the MCTDH implementation (N_{DVR} : number of DVR points, N_{SPF} : number of single particle functions) are given as well. Notice that modes q_2 and q_5 as well as q_3 and q_4 have been combined.

| mode | ω_i (cm^{-1}) | $\langle E^{(\text{reorg})} \rangle$ (cm^{-1}) | grid ($a_0(\text{a.m.u.})^{1/2}$) | N_{DVR} | N_{SPF} |
|-----------------|------------------------------------|--|--|------------------|------------------|
| q_1 (A_1) | 425 | 468 (72) | -7.5:7.5 | 45 | 10 |
| q_2 (A_1) | 1999 | 822 (122) | -1.7:1.7 | 25 | 10 |
| q_3 (E_2) | 2016 | 1426 (204) | -1.7:1.7 | 25 | 10 |
| q_4 (E_2) | 2016 | 1649 (239) | -1.7:1.7 | 25 | 10 |
| q_5 (A_1) | 2106 | 4646 (692) | -1.7:1.7 | 25 | 10 |

with the anharmonic coordinates to a seven-dimensional model. The bath mode parameters are compiled in Tab. III. Notice that the average reorganization energy depends, of course, on the grid size. In the table we report the average over the full grid as well as over a reduced grid onto which the wave packet will be mostly localized. The major effect on the dynamics of the \mathbf{Q} modes will come from the coupling to the other CO vibrations, not only because the forces are the largest, but also because of the near resonance. Among the lower-frequency modes only q_1 couples appreciably; it is a breathing mode of all equatorial CO groups with respect to the two Mn centers.

The molecular Hamiltonian is supplemented by the molecule-field interaction that is described in dipole approximation

$$H_{\text{field}}(t) = -\mathbf{d}(\mathbf{Q})\mathbf{E}(t), \quad (5)$$

where the dipole moment surfaces for the different polarization directions have been obtained along with the potential energy surface for the selected anharmonic degrees of freedom. Notice that within the approximation given by Eq. (4) there is no coupling to the other two IR active carbonyl modes (cf. Tab. II). Moreover, the latter are polarized in z -direction and will not be directly excited by the circularly polarized laser pulse. For the dynamics simulations it will be assumed that the molecule has been pre-oriented with the coordinate system as indicated in Fig. 1. The laser field will be taken to be of the form

$$\begin{aligned} \mathbf{E}(t) &= \begin{pmatrix} E_x(t) \\ E_y(t) \\ 0 \end{pmatrix} \\ &= E_0 \Theta(t) \Theta(t_p - t) \sin^2(\pi t/t_p) \begin{pmatrix} \cos(\omega t) \\ \sin(\omega t) \\ 0 \end{pmatrix}. \end{aligned} \quad (6)$$

Here t_p is the total pulse duration, ω the carrier frequency, and E_0 the field strength. These parameters

will be chosen such as to achieve the excitation of a vibrational superposition state with respect to the two E_1 modes, which corresponds to a wave packet performing a clockwise circulation on the potential energy surface $V(\mathbf{Q}, \mathbf{q} = 0)$. The respective normal mode displacements are shown in Fig. 2. Close inspection of this figure shows that during this circulation, the antisymmetric combination of stretching motions of equatorial CO groups which are opposite to each other "moves" around the symmetry (z) axis. Of course, this classical picture applies only as long as the wave packet stays compact and an important question to be addressed will be the regime of validity of this classical analogue.

The 7D time-dependent Schrödinger equation

$$i\hbar \frac{\partial}{\partial t} \Psi(\mathbf{Q}, \mathbf{q}; t) = [H_{\text{mol}} + H_{\text{field}}(t)] \Psi(\mathbf{Q}, \mathbf{q}; t) \quad (7)$$

has been solved using the MCTDH approach^{22,23} as implemented in the Heidelberg program package.³⁰ The seven-dimensional wave function $\Psi(\mathbf{Q}, \mathbf{q}; t)$ is represented on a grid in terms of a harmonic oscillator discrete variable representation (DVR). A total of 25 DVR points on the grid $[-1.7 : 1.7]a_0(\text{a.m.u.})^{1/2}$ together with 12 single particle functions (SPFs) are used for each of the \mathbf{Q} modes which are treated as a combined MCTDH particle. The parameters for the bath modes are compiled in Tab. III. Potential energy and dipole moment surfaces have been fitted on this grid using the POTFIT algorithm.²³ Using this set of SPFs the natural orbital populations have been below 10^{-5} . The actual propagation is performed using the variable mean field scheme with a 6th order Adams-Bashforth-Moulton integrator. The vibrational ground state, $|\Psi_0\rangle$, has been calculated using the improved relaxation scheme³¹; some uncoupled (one-dimensional zero-order) states in the \mathbf{Q} -subspace will be used for the discussion of the dynamics.

III. RESULTS AND DISCUSSION

In the following we will present results for the time-dependent wave packet dynamics which have been obtained for a carrier frequency ω , fixed to the fundamental transition of the E_1 modes, which is at 2014 cm^{-1} . The total propagation time has been set to 5 ps. First, we will discuss the effect of changing the field strength E_0 , before the variation of the pulse length is addressed. A global analysis of the dynamics will be given in terms of the following quantities: (i) the energy absorbed by the molecule at the end of the pulse: $\Delta E_{\text{mol}} = \langle \Psi(t_p) | H_{\text{mol}} | \Psi(t_p) \rangle - \langle \Psi_0 | H_{\text{mol}} | \Psi_0 \rangle$, (ii) the maximum energy change of the bath modes reached during the considered time interval of 5 ps: $\Delta E_{\text{bath}}^{(\text{max})} = \max(\langle \Psi(t) | H_{\mathbf{q}} | \Psi(t) \rangle - \langle \Psi_0 | H_{\mathbf{q}} | \Psi_0 \rangle)$, (iii) the maximum expectation value of the E_1 modes' coordinate operators during the 5 ps time interval: $Q^{(\text{max})} = \max(\langle \Psi(t) | \mathbf{Q} | \Psi(t) \rangle)$, and (iv) the population

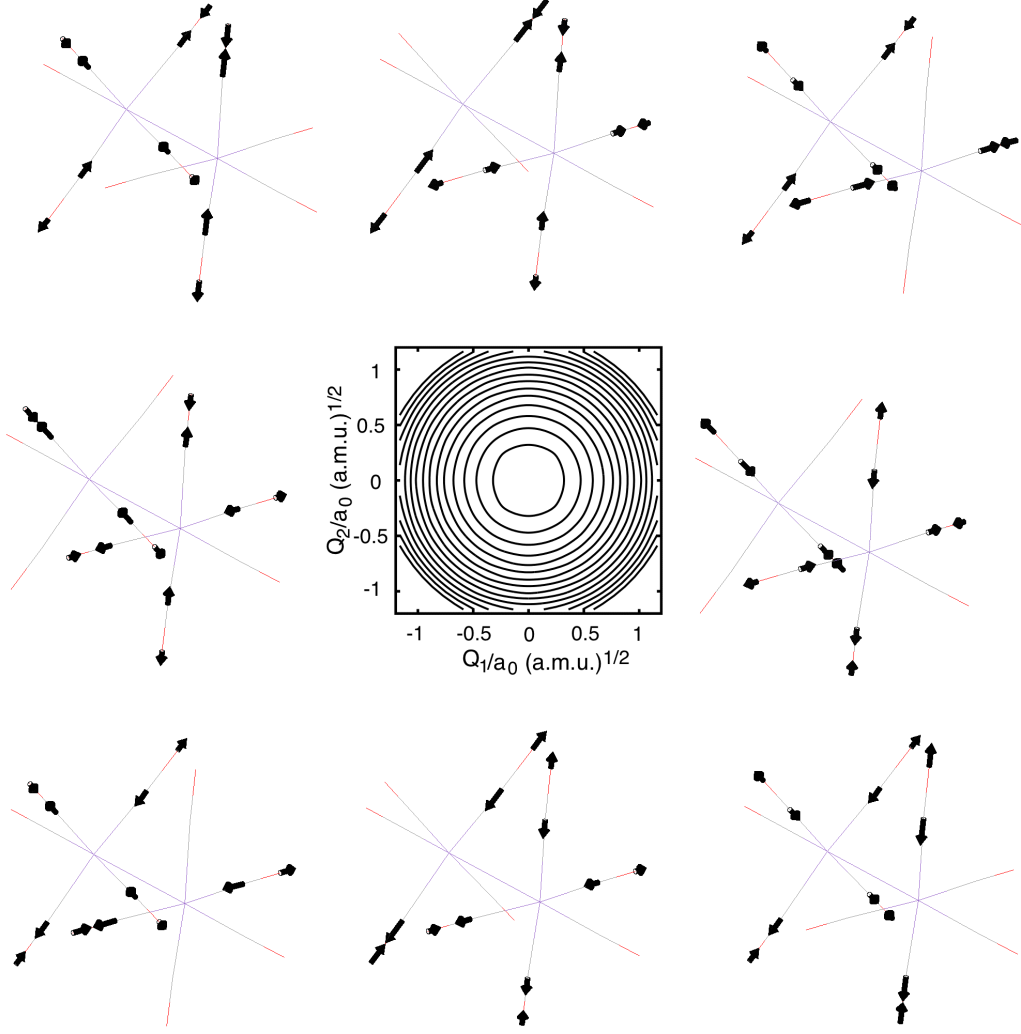


FIG. 2. Classical picture of vibrational wave packet circulation triggered by excitation of the two degenerate E_1 modes by means of a circularly polarized laser field. Shown are the displacement vectors for the superposition of the modes along a unit circle in steps of 45° . In the central panel the two-dimensional potential $V(\mathbf{Q}, \mathbf{q} = 0)$ is shown (contour lines in steps of 2000 cm^{-1} starting at 2000 cm^{-1}).

of the ground state at the end of the pulse: $P_0 = |\langle \Psi(t_p) | \Psi_0 \rangle|^2$.

A. Dependence on the Field Strength

A global analysis of the dynamics in dependence on the field strength and for a pulse duration of $t_p = 500 \text{ fs}$ is given in Tab. IV. Overall, we observe a monotonous decrease of the ground state population P_0 with increas-

ing field amplitude. For the highest amplitude used, the ground state is completely depopulated. At the same time the absorbed energy ΔE_{mol} increases, indicating vibrational ladder climbing. In fact for $E_0 = 1.5 \text{ mE}_h/ea_0$ the absorbed energy is compatible with an appreciable simultaneous population of the third vibrationally excited state in each of the two \mathbf{Q} modes. Analysis of the population shows that in fact many overtone and combination transitions are excited with the $(\nu_1 = 2, \nu_2 = 2)$ state having the largest population. For the more moderate

TABLE IV. Analysis of the laser-driven wave packet dynamics for a 500 fs pulse which is resonant to the fundamental transition of the E_1 modes (cf. Eq. (6)).

| E_0 (mE_h/ea_0) | ΔE_{mol} (cm^{-1}) | $\Delta E_{\text{bath}}^{(\text{max})}$ (cm^{-1}) | $Q^{(\text{max})}$ ($a_0\sqrt{\text{a.m.u}}$) | P_0 |
|---------------------------------|---|---|--|-------|
| 0.1 | 71 | 6 | 0.05 | 0.97 |
| 0.2 | 277 | 18 | 0.09 | 0.87 |
| 0.3 | 621 | 62 | 0.13 | 0.73 |
| 0.4 | 1099 | 164 | 0.18 | 0.57 |
| 0.5 | 1708 | 341 | 0.22 | 0.42 |
| 1.5 | 12733 | 4553 | 0.50 | 0.00 |

excitation with $E_0 = 0.5 \text{ mE}_h/ea_0$ the populations of the \mathbf{Q} modes' states is about 20% for (0,1) and (0,1), 8% for (1,1) and 4 % for (2,0) and (0,2).

The anharmonic coupling to the bath modes will increase along with the absorbed energy, i.e. if the wave packet explores configurations away from equilibrium. For moderate excitation conditions the extent of anharmonic coupling is rather small, e.g. if the amount of absorbed energy corresponds to about one quantum of excitation in a CO mode ($E_0 = 0.5 \text{ mE}_h/ea_0$) we find $\Delta E_{\text{mol}}/\Delta E_{\text{bath}}^{(\text{max})} \approx 5$. The effect of the bath becomes appreciable only under high excitation conditions, e.g., for $E_0 = 1.5 \text{ mE}_h/ea_0$ we find $\Delta E_{\text{mol}}/\Delta E_{\text{bath}}^{(\text{max})} \approx 2.8$. In Fig. 3 we show the expectation values of the Hamiltonian operators for the system modes, $H_{\mathbf{Q}}$, and the uncoupled bath modes, $H_{\mathbf{q}}$, for two field strengths. As expected the energy of the \mathbf{Q} modes rises during laser pulse excitation ($t_p = 500$ fs) as seen in panel (a). For the lower field strength the expectation value subsequently oscillates around the attained value signaling reversible energy exchange with the bath modes. Indeed the corresponding oscillations in the bath mode energies are seen in panel (b). Increasing the field strength, the energy exchange with the bath is more pronounced and instead of regular oscillations the onset of equilibration among the bath modes is observed in panel (c). Still there is no appreciable coupling to lower frequency modes that could lead to an energy flow out of the selected \mathbf{Q} modes. We notice from panels (b) and (c) that the low-frequency mode q_1 , which was selected because it had the largest reorganization energy in the lower-frequency part of the spectrum is not appreciably excited. Finally, we comment on the initial partitioning of energy among the bath modes. Inspecting Tab. III one might have anticipated that mode q_5 will dominate the bath dynamics. However, the fundamental frequency of the laser-excited \mathbf{Q} modes is 2014 cm^{-1} , which is resonant to $q_2 - q_4$, but rather off-resonant with respect to q_5 . Hence, energy exchange between the \mathbf{Q} and the q_5 modes is not very efficient.

The focus of the present investigation is on the wave packet circulation with respect to the E_1 modes. Inspecting Tab. IV we notice that the maximum bond elongation increases with the amount of absorbed energy. The

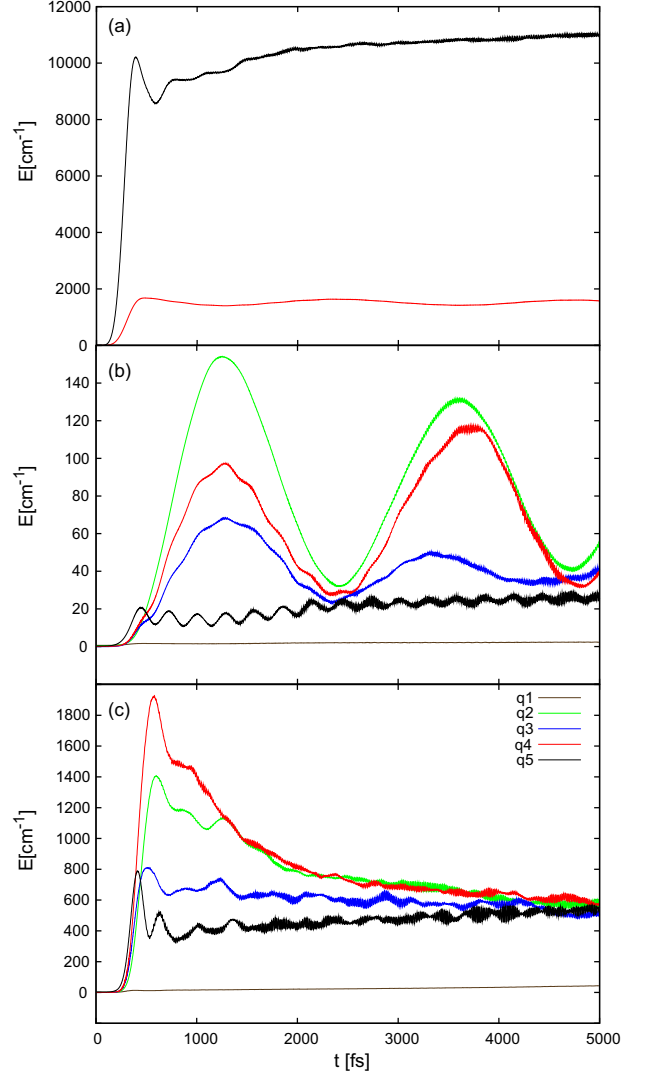


FIG. 3. (a) Expectation values of $H_{\mathbf{Q}}$ for a 500 fs excitation with field strength $E_0 = 0.5 \text{ mE}_h/ea_0$ (lower curve) and $1.5 \text{ mE}_h/ea_0$ (upper curve). The respective expectation values of $H_{\mathbf{q}}$ for the five bath modes are shown in panels (b) ($E_0 = 0.5 \text{ mE}_h/ea_0$) and (c) ($E_0 = 1.5 \text{ mE}_h/ea_0$). With increasing energy at about 1000 fs the curves correspond to q_1 , q_5 , q_3 , q_2 , and q_4 in panel (c), whereas in panel (b) q_2 and q_4 are interchanged (see also key in panel (c)).

value that is reached can be compared, e.g., with the variance of the ground state coordinate distribution which is $0.17 a_0\sqrt{\text{a.m.u}}$ for the \mathbf{Q} modes. Thus for the largest field strength we observe that the bond elongation is about three times this ground state variance. A more detailed picture is provided by inspecting the coordinate operator expectation values, $Q_i(t) = \langle \Psi(t) | Q_i | \Psi(t) \rangle$, which are shown in Fig. 4. In the parametric plot the expectation values trace a clockwise circulating trajectory on the potential $V(\mathbf{Q}, \mathbf{q} = \mathbf{0})$. For small field strengths the amplitude of this circulation increases during the excitation

TABLE V. Analysis of the laser-driven wave packet dynamics for pulses of different duration and amplitude. The integrated field envelope is identical in all cases.

| t_p (fs) | E_0 (mE_h/ea_0) | ΔE_{mol} (cm^{-1}) | $\Delta E_{\text{bath}}^{(\text{max})}$ (cm^{-1}) | $Q^{(\text{max})}$ ($a_0\sqrt{\text{a.m.u}}$) | P_0 |
|---------------|---------------------------------|---|---|--|-------|
| 100 | 2.5 | 1812 | 374 | 0.23 | 0.40 |
| 500 | 0.5 | 1708 | 341 | 0.22 | 0.42 |
| 1000 | 0.25 | 1441 | 273 | 0.20 | 0.47 |
| 1500 | 0.17 | 1146 | 205 | 0.18 | 0.54 |

period of 500 fs (upper and middle panel of Fig. 4). For the strongest field used (lower panel of Fig. 4) the amplitude of the circulation starts to decrease already during the interaction with the pulse. Furthermore, after the excitation pulse is over the behavior shows a strong dependence on the field amplitude (right column of Fig. 4). Judging from the amount of energy redistribution given in Tab. IV the decrease of $Q_i(t)$ can only in part be an effect of the anharmonic coupling to the bath. Instead it is the wave packet dispersion that is mostly responsible for this decrease of $Q_i(t)$. This is shown in Fig. 5 where snapshots of the reduced density are plotted for the case of $E_0 = 0.5 \text{ mE}_h/ea_0$. One notices that the wave packet stays compact in the excitation period only, but then starts to disperse. Eventually, the wave packet is rather delocalized even though it is still circulating. However, due to the delocalization negative and positive coordinate values contribute to the expectation values along the \mathbf{Q} axes and therefore the expectation values become smaller and cannot reflect the wave packet circulation anymore. With increasing excitation more eigenstates contribute to the wave packet such that the dispersion effect becomes more pronounced and sets in already during the pulse.

B. Dependence on the Pulse Duration

In the following we investigate the dependence of the laser-driven wave packet dynamics on the duration of the excitation pulse. As a reference case we have used $t_p = 500$ fs and $E_0 = 0.5 \text{ mE}_h/ea_0$. For a given duration t_p the field amplitudes have been chosen such as to keep the integrated field envelope at the same value as in the reference case. Note that we are not dealing with a two level system and that the pulses are no π -pulses. The pulse parameters are summarized in Tab. V.

Table V also contains the various expectation values, which give a global characterization of the dynamics. First, we notice that the different pulse durations give comparable depopulations of the vibrational ground state between 40 and 54%. The amount of energy absorbed by the molecule decreases with the pulse duration and is largest for the shortest pulse ($t_p = 100$ fs), although the difference to the reference pulse is only 6%. At the same time the excitation of bath modes decreases from a con-

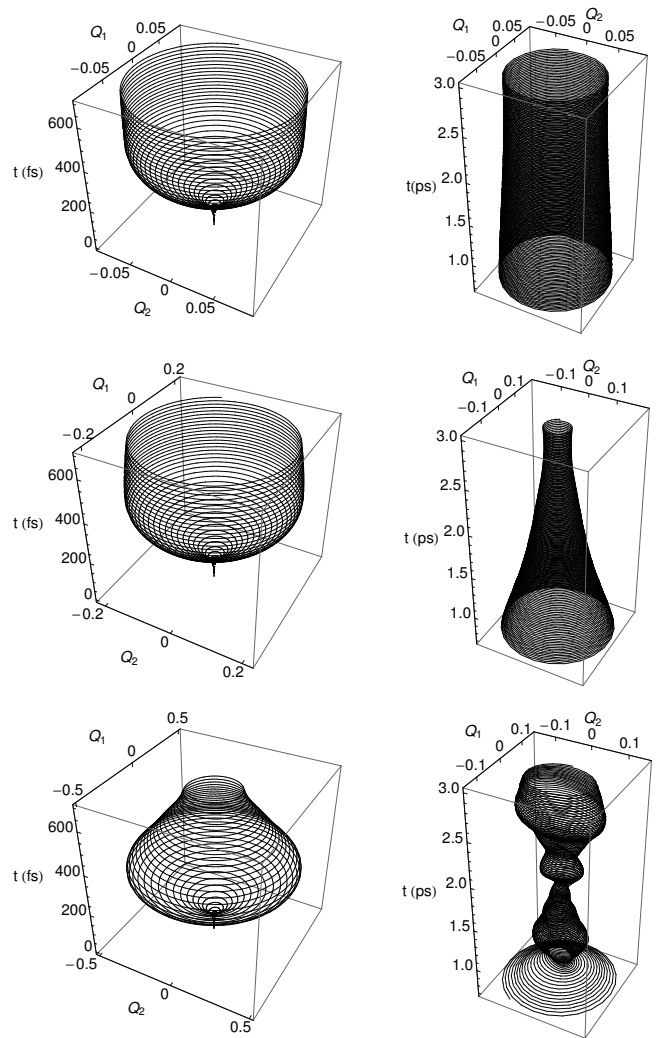


FIG. 4. Parametric plots of (Q_1, Q_2) (in $a_0\sqrt{\text{a.m.u}}$) for a 500 fs laser pulse excitation and a field strength E_0 (in mE_h/ea_0) of 0.2 (upper row), 0.5 (middle row) and 1.5 (bottom row). (Notice the different axes scales).

tribution to the total energy of 21% for $t_p = 100$ fs down to 18% for $t_p = 1500$. Moreover, the maximum radius of circulation of the expectation value of the \mathbf{Q} coordinates is reduced slightly. Inspecting the time dependence of the $Q_i(t)$ in Fig. 6 we notice that again we have an initial period, where the wave packet stays rather compact such that the coordinate expectation values give a reasonable picture of the moving wave packet. This is followed by a period where the wave packet disperses such that the dynamics cannot be understood from the expectation values. As far as the pulse duration dependence is concerned the most striking observation from Fig. 6 is that the time span of compact wave packet propagation can be prolonged by increasing the parameter t_p . In passing we note that this does also imply that the time span of circulation at about the full radius is longer, but of course not identical to t_p . For $t_p = 500$ fs and 1500

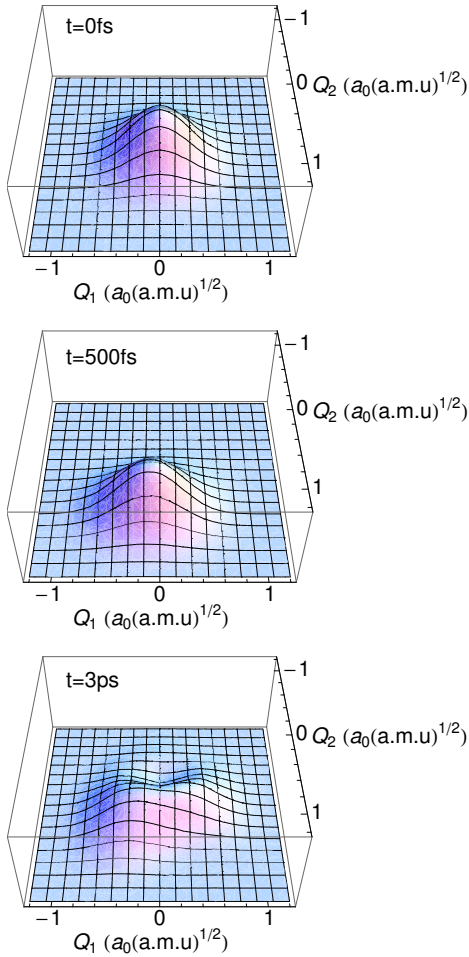


FIG. 5. Snapshots of the time evolution of the reduced density with respect to the \mathbf{Q} modes for laser-driving with a pulse having the parameters $t_p = 500$ fs, $E_0 = 0.5$ mE_h/ea₀, and $\omega/2\pi c = 2014$ cm⁻¹.

fs the expectation values $Q_i(t)$ are within 90% of their maximum value during the interval [450 : 800] fs and [950 : 1650] fs, respectively. Since the anharmonic coupling is still small in the considered range of the potential energy surface corresponding to about one to two quanta of excitation of the E_1 modes, intramolecular energy redistribution doesn't destroy wave packet circulation even for the longest pulse duration of 1.5 ps and subsequent 3.5 ps free evolution.

IV. SUMMARY

We have demonstrated laser-driven wave packet circulation with respect to the two degenerate E_1 carbonyl stretching vibrations in a pre-oriented Mn₂(CO)₁₀ model. The wave packet circulation corresponds to a vibrational excitation moving around

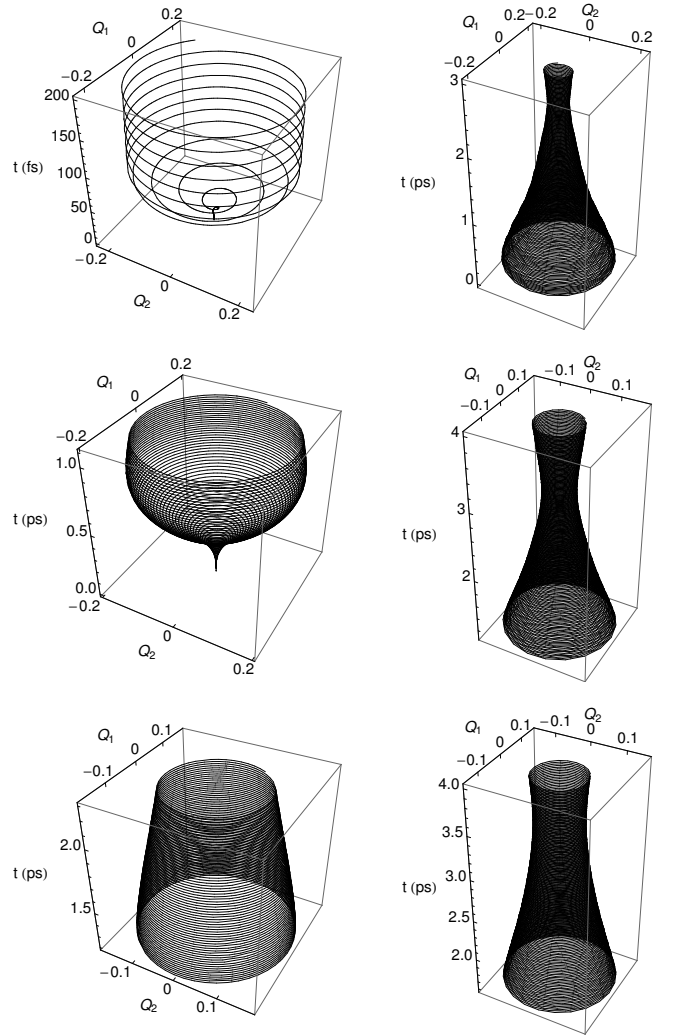


FIG. 6. Parametric plots of (Q_1, Q_2) (in $a_0\sqrt{\text{a.m.u}}$) for different pulse durations. Upper row: $t_p = 100$ fs, $E_0 = 2.5$ mE_h/ea₀, middle row: $t_p = 1000$ fs, $E_0 = 0.25$ mE_h/ea₀, bottom row: $t_p = 1500$ fs, $E_0 = 0.17$ mE_h/ea₀. (Notice the different axes scales).

the symmetry axis of the system. It has been shown that a classical picture holds approximately during the interaction with the excitation laser pulse. Later on, appreciable wave packet dispersion sets in such that the classical picture becomes meaningless, although the wave packet still circulates around the minimum of the potential energy surface.

The possibility of wave packet circulation upon excitation of degenerate vibrational modes with circularly polarized laser light could have been anticipated from the work of J. Manz et al. on triatomic molecules.^{5,6} Therefore, the most important result of the present study concerns the robustness of wave packet circulation with respect to intramolecular vibrational energy redistribution in a polyatomic molecule. To proof this we have considered the coupling of the two E_1 mode to other in-

tramolecular degrees of freedom, which have been described in harmonic approximation. This resulted in a seven-dimensional model for which the time-dependent Schrödinger equation has been solved using the MCTDH approach. For moderate excitation conditions of one or two quanta in the E_1 modes, at most about 20 % of the absorbed energy is disposed into the bath modes within a time span of 5 picoseconds. This finding appears to be encouraging and should stimulate experimental verification.

ACKNOWLEDGMENT

We gratefully acknowledge financial support from the Deutsche Forschungsgemeinschaft (project Ku952/6-1).

- ¹I. Barth and J. Manz. *Angew. Chem. Int. Ed.* **45**, 2962 (2006).
- ²I. Barth, J. Manz, Y. Shigeta, and K. Yagi. *J. Am. Chem. Soc.* **128**, 7043 (2006).
- ³I. Barth, J. Manz, and L. Serrano-Andres. *Chem. Phys.* **347**, 263 (2008).
- ⁴I. Barth and J. Manz. *Phys. Rev. A* **75**, 012510 (2007).
- ⁵I. Barth, J. Manz, and P. Sebal. *Chem. Phys.* **346**, 89 (2008).
- ⁶I. Barth, J. Manz, G. Perez-Hernandez, and P. Sebal. *Z. Phys. Chem.* **222**, 1311 (2008).
- ⁷J. Gaus, K. Kobe, V. Bonačić-Koutecký, H. Kühling, J. Manz, B. Reischl, S. Rutz, E. Schreiber, and L. Wöste. *J. Phys. Chem.* **97**, 12509 (1993).
- ⁸V. May and O. Kühn. *Charge and Energy Transfer Dynamics in Molecular Systems, 3rd revised and enlarged edition* (Wiley-VCH, Weinheim, 2011).
- ⁹S. Arrivo, T. Dougherty, W. Grubbs, and E. Heilweil. *Chem. Phys. Lett.* **235**, 247 (1995).
- ¹⁰T. Witte, T. Hornung, L. Windhorn, D. Proch, R. de Vivie-Riedle, M. Motzkus, and K. L. Kompa. *J. Chem. Phys.* **118**, 2021 (2003).
- ¹¹C. Ventalon, J. M. Fraser, M. H. Vos, A. Alexandrou, J.-L. Martin, and M. Joffre. *Proc. Natl. Acad. Sci. USA* **101**, 13216 (2004).
- ¹²C. Meier and M.-C. Heitz. *J. Chem. Phys.* **123**, 044504 (2005).
- ¹³O. Kühn. *Chem. Phys. Lett.* **402**, 48 (2005).
- ¹⁴O. Kühn. In *Multidimensional Quantum Dynamics* (edited by H.-D. Meyer, F. Gatti, and G. A. Worth) (Wiley-VCH, Weinheim, 2009), p. 329.
- ¹⁵C. Gollub, B. M. R. Korff, K. L. Kompa, and R. de Vivie-Riedle. *Phys. Chem. Chem. Phys.* **9**, 369 (2007).
- ¹⁶D. B. Strasfeld, S.-H. Shim, and M. T. Zanni. *Phys. Rev. Lett.* **99**, 038102 (2007).
- ¹⁷O. Kühn, M. R. D. Hachey, M. M. Rohmer, and C. Daniel. *Chem. Phys. Lett.* **322**, 199 (2000).
- ¹⁸M. J. Nee, C. R. Baiz, J. M. Anna, R. Mccanne, and K. J. Kubarych. *J. Chem. Phys.* **129**, 084503 (2008).
- ¹⁹C. R. Baiz, P. L. McRobbie, N. K. Preketes, K. J. Kubarych, and E. Geva. *J. Phys. Chem. A* **113**, 9617 (2009).
- ²⁰C. R. Baiz, P. L. McRobbie, J. M. Anna, E. Geva, and K. J. Kubarych. *Acc. Chem. Res.* **42**, 1395 (2009).
- ²¹J. T. King, C. R. Baiz, and K. J. Kubarych. *J. Phys. Chem. A* **114**, 10590 (2010).
- ²²H.-D. Meyer, U. Manthe, and L. S. Cederbaum. *Chem. Phys. Lett.* **165**, 73 (1990).
- ²³M. H. Beck, A. Jäckle, G. A. Worth, and H.-D. Meyer. *Phys. Rep.* **324**, 1 (2000).
- ²⁴M. J. Frisch, G. W. Trucks, H. B. Schlegel, G. E. Scuseria, M. A. Robb, J. R. Cheeseman, J. Montgomery, T. Vreven, K. N. Kudin, J. C. Burant, J. M. Millam, S. S. Iyengar, J. Tomasi, V. Barone, B. Mennucci, M. Cossi, G. Scalmani, N. Rega, G. A. Petersson, H. Nakatsuji, M. Hada, M. Ehara, K. Toyota, R. Fukuda, J. Hasegawa, M. Ishida, T. Nakajima, Y. Honda, O. Kitao, H. Nakai, M. Klene, X. Li, J. E. Knox, H. P. Hratchian, J. B. Cross, V. Bakken, C. Adamo, J. Jaramillo, R. Gomperts, R. E. Stratmann, O. Yazyev, A. J. Austin, R. Cammi, C. Pomelli, J. W. Ochterski, P. Y. Ayala, K. Morokuma, G. A. Voth, P. Salvador, J. J. Dannenberg, V. G. Zakrzewski, S. Dapprich, A. D. Daniels, M. C. Strain, O. Farkas, D. K. Malick, A. D. Rabuck, K. Raghavachari, J. B. Foresman, J. V. Ortiz, Q. Cui, A. G. Baboul, S. Clifford, J. Cioslowski, B. B. Stefanov, G. Liu, A. Liashenko, P. Piskorz, I. Komaromi, R. L. Martin, D. J. Fox, T. Keith, M. A. Al-Laham, C. Y. Peng, A. Nanayakkara, M. Challacombe, P. M. W. Gill, B. Johnson, W. Chen, M. W. Wong, C. Gonzalez, and J. A. Pople. *Gaussian 03, Revision B.04*. Wallingford, CT (2004).
- ²⁵L. Dahl and R. Rundle. *Acta Crystallogr.* **16**, 419 (1963).
- ²⁶A. Almenningen, G. G. Jacobsen, and H. M. Seip. *Acta Chem. Scand.* **23**, 685 (1969).
- ²⁷M. Martin, B. Rees, and A. Mitschler. *Acta Crystallogr. B* **38**, 6 (1982).
- ²⁸H. Haas and R. K. Sheline. *J. Chem. Phys.* **47**, 2996 (1967).
- ²⁹D. J. Parker. *Spectrochim. Acta A* **39**, 463 (1983).
- ³⁰G. Worth, M. Beck, A. Jäckle, and H.-D. Meyer. *The MCTDH Package*, Version 8.2 (2000) University of Heidelberg, Heidelberg, H.-D. Meyer, Version 8.3 (2002), Version 8.4 (2007).
- ³¹H.-D. Meyer, F. L. Quere, C. Leonard, and F. Gatti. *Chem. Phys.* **329**, 179 (2006).